Aalborg Universitet

Low Voltage Ride-Through of Two-Stage Grid-Connected Photovoltaic Systems Through the Inherent Linear Power-Voltage Characteristic

Yang, Yongheng; Sangwongwanich, Ariya; Liu, Hongpeng; Blaabjerg, Frede

Low Voltage Ride-Through of Two-Stage Grid-Connected Photovoltaic Systems Through the Inherent Linear Power-Voltage Characteristic

Yongheng Yang*, *Member, IEEE,* Ariya Sangwongwanich*, *Student Member, IEEE,*

Hongpeng Liu†, *Member, IEEE,* and Frede Blaabjerg*, *Fellow, IEEE*

*Department of Energy Technology, Aalborg University, Aalborg 9220, Denmark
†Department of Electrical Engineering, Harbin Institute of Technology, Harbin 150001, China
yoy@et.aau.dk; ars@et.aau.dk; lhp602@hit.edu.cn; fbl@et.aau.dk

Abstract—In this paper, a cost-effective control scheme for two-stage grid-connected PhotoVoltaic (PV) systems in Low Voltage Ride-Through (LVRT) operation is proposed. In the case of LVRT, the active power injection by PV panels should be limited to prevent from inverter over-current and also energy aggregation at the dc-link, which will challenge the dc-link capacitor lifetime if remains uncontrolled. At the same time, reactive currents should be injected upon any demand imposed by the system operators. In the proposed scheme, the two objectives can be feasibly achieved. The active power is regulated automatically through a proportional controller according to the voltage sag level and PV inherent characteristics (i.e., the voltage and power droop). Compared to prior-art LVRT schemes, the proposed method is cost-effective, as it is achieved by simply plugging the proportional controller into a maximum power point tracking controller without significant hardware or software modifications. In this way, the PV system will not operate at the maximum power point, whereas the inverter will not face any over-current challenge but can provide reactive power support in response to the grid voltage fault. Simulations have been performed on a 3-kW two-stage grid-connected single-phase PV system in the case of LVRT operation, where the results have verified the proposed control scheme in terms of fast dynamics and seamless operation mode transitions.

Index Terms—Low voltage ride-through; active power control; grid-connected photovoltaic (PV) systems; droop characteristics; maximum power point tracking; two-stage PV systems.

I. Introduction

Advanced functionalities that can be provided by grid-connected PhotoVoltaic (PV) systems are becoming of high demand in some countries [1]–[4]. Commonly, it can be summarized that in most cases the PV systems should be multi-functional as an active player to participate in grid regulation beyond solely generating energy [3], [5]–[9]. For instance, the Low Voltage Ride-Through (LVRT) capability in response to grid voltage sags has been extended as one

ancillary service to grid-connected PV systems. Currently, this functionality can be seen in three-phase PV systems [7]–[17], single-phase PV systems [6], [18], [19] and even PV modules [20]. At the beginning, this LVRT demand was only for wind power systems, where due to large physical inertia, additional devices (e.g., dc-chopper or crowbar) are required for power dissipation during the LVRT operation [21]. Although PV systems are still connected to low-voltage and medium-voltage level networks and do not have much physical inertia, the excessive energy should also be taken care of in the case of fault ride-through operation; otherwise, it may cause the dc-link voltage go excursion as well as over-current since the energy will aggregate at the dc-link [22]. Following, it may trigger the system protection scheme, leading to a failure of LVRT operation (or even system collapse).

Thus, many LVRT schemes have been developed in literature for both three-phase and single-phase grid-connected PV systems. For three-phase systems, the presence of positive- and negative-sequence voltages/currents under grid faults should be properly coped with, which in return also provides much flexibility for power injections during LVRT [8], [11]–[16]. For instance, a peak current limit control scheme which can inject the required current and negative sequence current was employed in [12] also to suppress the negative sequence grid voltages during LVRT. In contrast, there are fewer control variables (i.e., grid voltage and current) in single-phase grid-connected PV systems, and thus the control becomes challenging under low voltage faults. Nevertheless, as a general and intuitive approach, a control switching unit is employed to directly change the operational mode from the Maximum Power Point Tracking (MPPT) with unity power factor to LVRT with reactive power injection, once a voltage fault is detected. For example, in [11], [14] and [18], when an instantaneous fault is identified, the reference signals will be generated instantaneously, which may induce large overshoots. Thus, it calls for advanced control schemes that should enable a smooth operation transition. Additionally, the PV panel dynamics are rarely considered in these LVRT schemes, which however may affect the entire system performance.
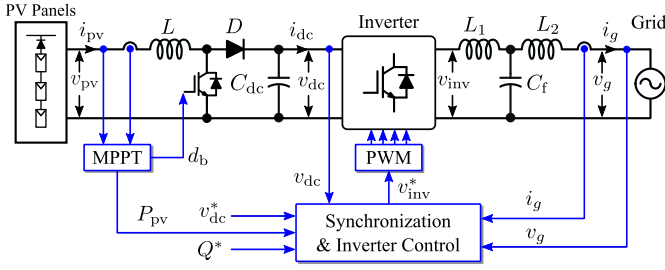
Fig. 1. Schematic and overall control structure of a single-phase two-stage grid-connected PV system with an LCL filter.
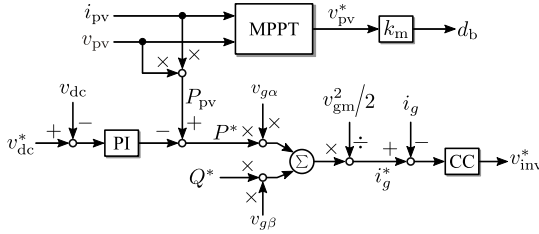

Fig. 2. Detailed control structure of the single-phase two-stage grid-connected PV system (CC - Current Controller with harmonic compensation), where v_{gm} is the instantaneous amplitude of the grid voltage.

In light of the above, this paper proposes a cost-effective LVRT scheme for two-stage single-phase PV systems in § II. The proposed solution adopts a simple proportional controller designed according to the grid voltage sag level and the inherent *power-voltage* characteristics of the PV panels, and it is plugged into an MPPT controller. Hence, it enables a seamless operation mode transition with fast dynamics. Simulations have been performed on a 3-kW two-stage grid-connected single-phase PV system to verify the proposed LVRT scheme. Results are presented in § III. Finally, concluding remarks are provided in § IV.

II. PROPOSED LOW VOLTAGE RIDE-THROUGH STRATEGY

A. Control of Two-Stage Single-Phase PV Systems

Since the power ratings of string PV inverters are of up to 6 kW, it is common to connect the PV systems to single-phase feeders using a two-stage configuration [23], [24]. In this sense, the proposed LVRT scheme is described and demonstrated on a single-phase system, which as mentioned has two stages: a dc-dc boost stage and a dc-ac inversion stage. Fig. 1 shows the configuration of the two-stage single-phase PV system and its overall control structure. Notably, the boost converter not only enables a flexible active power control but also extends the system operating hours (i.e., the PV system can still feed power into the grid under very weak solar irradiance). Accordingly, the MPPT control is implemented in the control of the boost stage as shown in Fig. 2, where k_m is the MPPT control gain.

For the inverter control, a cascaded dual-loop controller is adopted, where the outer loop controls the dc-link voltage v_{dc} through a Proportional Integral (PI) controller with the feed-forwarded PV power P_{pv}. Then, the reference i_g^* for the inner

loop current controller of the dual-loop control structure is generated according to the single-phase PQ theory [18], as it is shown in Fig. 2. The PI controller ($G_{PI}(s)$) for the dc-link voltage can be expressed as

$$G_{PI}(s) = k_p + \frac{k_i}{s} \qquad (1)$$

in which k_p and k_i are the proportional and integral control gain, respectively. Moreover, it should be noted that, in Fig. 2, $v_{g\alpha} = v_g$, and $v_{g\beta}$ is a virtual voltage that is in-quadrature with the real grid voltage v_g, and

$$v_{gm} = \sqrt{v_{g\alpha}^2 + v_{g\beta}^2} \qquad (2)$$

being the grid voltage amplitude. In addition, the Current Controller (CC) like a Proportional Resonant (PR) controller and a dead beat controller that work in the $\alpha\beta$ reference frame can be adopted, and also in consideration of the current quality, harmonic compensation like Multiple Parallel Resonant Controllers (MPRC) and a Repetitive Controller (RC) can be employed [21], [25]. In this paper, a PR controller ($G_{PR}(s)$) has been used as the fundamental-frequency current controller, and an RC ($G_{RC}(s)$) has been employed to compensate the harmonics. The entire CC can then be given as

$$\begin{aligned} G_{CC}(s) &= G_{PR}(s) + G_{RC}(s) \\ &= k_{pr} + \frac{k_{ir}}{s^2 + \omega_0^2} + \frac{k_{rc}Q(s)e^{-sT_0}}{1 - Q(s)e^{-sT_0}} \cdot G_f(s) \end{aligned} \qquad (3)$$

where k_{pr} and k_{ir} are the proportional and resonant control gain for the PR controller, respectively, with ω_0 being the fundamental grid frequency; k_{rc} is the control gain for the RC with $T_0 = 2\pi/\omega_0$ being the fundamental period, $Q(s)$ is a low pass filter, and $G_f(s) = e^{sT_c}$ is a phase-lead compensator with T_c being the compensation time [25]. Notably, $Q(s)$ and $G_f(s)$ can enhance the controller robustness.

B. Proposed Low Voltage Ride-Through Strategy

As mentioned previously, in the case of LVRT, the PV system has to reduce its active power injection but to provide reactive power; otherwise, the PV inverter may experience over-current. In practice, the single-phase PV systems (with the rated power typically below 6 kW) are connected to low voltage feeders with a large *R/X* ratio, meaning that the grid is mainly resistive. In that case, the injected active power P_g has a droop relationship with the grid voltage level v_{gm} [26], [27] that is represented by

$$v_{gm} = v_{gm}^0 - k_d \left(P_g - P_g^0 \right) \qquad (4)$$

in which k_d is the active power droop coefficient, P_g is the injected active power, and the superscript "0" denotes the initial value. It should be noted that the droop controller in (4) is not used in the control of the two-stage grid-connected PV system shown in Fig. 2. Here, only is it used to demonstrate the droop characteristic between the grid voltage amplitude and the injected active power.

Additionally, according to the *Power-Voltage* (*P-V*) characteristics of the PV panels shown in Fig. 3, the PV output power
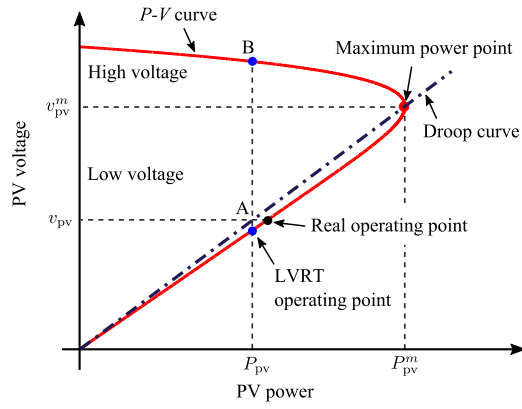
Fig. 3. *Power-Voltage* (*P-V*) characteristic of the PV panels and the theoretical (ideal) operating point (A or B) for the PV panels of two-stage grid-connected PV systems in the case of LVRT, where v_{pv} and P_{pv} are the PV voltage and power, respectively, with the superscript "m" denoting the voltage and power at the maximum power point.

also inherently has an approximately linear droop relationship with the PV voltage in the low voltage region. The inherent linear droop relationship can be expressed as

$$v_{pv} \approx v_{pv}^m + k_{pv} \left(P_{pv} - P_{pv}^m \right) \qquad (5)$$

where v_{pv} and P_{pv} are the PV voltage and power, respectively, k_{pv} is the *P-V* droop coefficient, and m represents the PV voltage and power at the maximum power point (can be obtained from the MPPT unit).

When assuming that the power losses are negligible (i.e., $P_g \approx P_{pv}$ in steady-state) and according to (4) and (5), the grid voltage level deviation Δv_{gm} is proportional to the changes of the PV voltage Δv_{pv} as

$$\Delta v_{gm} \approx -\frac{k_d}{k_{pv}} \Delta v_{pv} \qquad (6)$$

with $\Delta v_{gm} = v_{gm} - v_{gm}^0$ and $\Delta v_{pv} = v_{pv} - v_{pv}^m$. Clearly, in the normal operation mode, the grid voltage amplitude is almost constant at the nominal value (i.e., $v_{gm} = v_{gm}^0$), and hence, the PV voltage will be maintained by the MPPT controller (i.e., $v_{pv} = v_{pv}^m$). In that case, the PV voltage reference is the MPPT controller output as $v_{pv}^* = v_{pv}^m$. By contrast, in the case of LVRT, the grid voltage level reduces, and $\Delta v_{gm} \neq 0$. Thus, it is straightforward to maintain the voltage relationship in (6) so that a seamless operational mode transition is ensured. That is to say, the active power of the PV panels will be automatically regulated in the case of LVRT. According to (6), the PV voltage reference should be adjusted as

$$v_{pv}^* = v_{pv}^m - k\Delta v_{gm} = v_{pv}^m - k \left(v_{gm} - v_{gm}^0 \right) \qquad (7)$$

in which $k = k_{pv}/k_d$ is the control gain for the proposed strategy and v_{pv}^m is obtained from the MPPT controller. Compared to the control of the boost converter in the normal operation mode, the proposed LVRT control scheme for the boost converter simply plugs in a proportional controller (i.e., the control gain is k). Fig. 4 then shows the boost converter control structure of the proposed LVRT scheme.
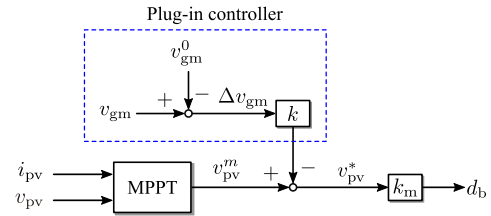

Fig. 4. Implementation of the proposed LVRT scheme plug-in the MPPT control of the boost converter for two-stage grid-connected PV systems.

Clearly, as shown in Fig. 3, there are two LVRT possibilities for the PV voltages, i.e., Point A corresponding to a low voltage in the region of low dP_{pv}/dv_{pv} and Point B corresponding to a high voltage in the region of high dP_{pv}/dv_{pv}. The PV system can be controlled at both points, depending on the polarity of the gain k. If the PV system is controlled to operate at Point A in LVRT mode, the PV power variation will be smaller compared to that when operating at Point B. As a consequence, the PV system has been controlled to operate at Point A, where thus the control gain k should be positive. According to Fig. 4, the voltage sag will increase the PV voltage reference v_{pv}^*, corresponding to an increase of the duty-cycle d_b. Hence, the PV voltage v_{pv} will be moved to the left side of the maximum power point in practice.

C. Parameter Design Considerations

Under normal grid conditions (i.e., $v_{gm} = v_{gm}^0$), the output of the plug-in LVRT scheme will be null according to (7) and Fig. 4, meaning that the PV system is operating at MPPT mode. However, when a grid voltage sag occurs (i.e., $v_{gm} < v_{gm}^0$), the proposed LVRT control scheme will automatically adjust the PV reference voltage v_{pv}^* according to (7), and thus the PV output power will be regulated to a lower level (i.e., Point A in Fig. 3), as aforementioned. Once the grid voltage fault is cleared (i.e., the voltage level recoveries), the proposed plug-in LVRT scheme will seamlessly change the operation mode back to the MPPT mode.

For the controller design, since a seamless operational mode transition is ensured, the MPPT control gain k_m can be designed when considering the system without the plug-in LVRT control scheme. This became a conventional design issue for a MPPT controller (e.g., a Perturb and Observe - P&O method), which is not the focus of this paper. Hence, the design of the MPPT controller is directed to [28]–[30]. In this sense, the proposed LVRT control scheme is simple, since only the droop coefficients (i.e., k_d and k_{pv}) have to be determined. Actually, the *P-V* droop coefficient k_{pv} is already fixed by the panel specifications and system operating conditions (i.e., ambient temperature and solar irradiance), as exemplified in Fig. 5. More specific, the *P-V* droop coefficient k_{pv} can be calculated as

$$k_{pv} = \frac{v_{pv}^m}{P_{pv}^m}. \qquad (8)$$

It is clear that this droop coefficient can be updated according to the MPPT controller (i.e., the outputs: v_{pv}^m and P_{pv}^m).
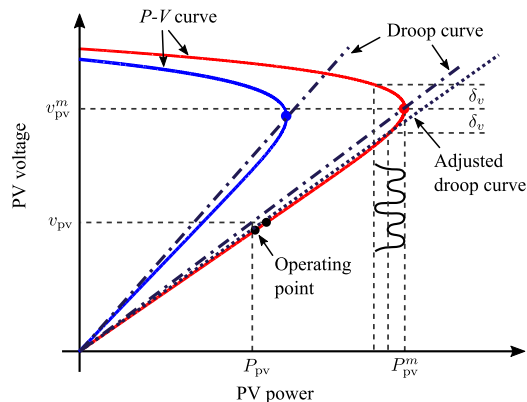
Fig. 5. Relationship between the *P-V* droop coefficient k_{pv} for the proposed LVRT scheme and the operating conditions, i.e., weak solar irradiance (blue) and strong solar irradiance (red) with a constant ambient temperature, where δ_v is the perturbation step-size of the MPPT controller (e.g., the P&O MPPT method).

However, as it is shown in Figs. 3 and 5, approximating the droop coefficient using the MPPT outputs will result in an inaccurate voltage reference. That is to say, the real operating point in LVRT will be slightly shifted towards the maximum power point (see Fig. 3). In order to alleviate this impact, the *P-V* droop coefficient obtained from (8) should be adjusted. Considering the most commonly-used MPPT scheme (i.e., the P&O MPPT method) [30], the adjustment can be achieved as shown in Fig. 5 and given by

$$k_{pv} = \frac{v_{pv}^m - \delta_v}{P_{pv}^m} \tag{9}$$

where δ_v is the perturbation step-size of the P&O MPPT controller. Notably, since there will be oscillations in the PV output power as indicated in Fig. 5 and also the output voltage (due to perturbation), the voltage and power at the maximum power point in (9) should be taken from averaged data (at least three samples) for higher accuracy. It is also worth noticing that an accurate droop coefficient may be attained through advanced estimation techniques like a quadrature curve-fitting method in [31] and a complete modeling of the PV characteristic curves as it is in [32]. Alternatively, corrections can be programmed as a look-up table, which simplifies practical implementations. Nevertheless, the *P-V* droop coefficient k_{pv} is fixed but it can be obtained following the above analysis.

Substituting (9) into (7) yields

$$v_{pv}^* = v_{pv}^m - \frac{v_{pv}^m - \delta_v}{k_d P_{pv}^m}(v_{gm} - v_{gm}^0) \tag{10}$$

which implies that only the active power droop coefficient k_d has to be designed in the proposed LVRT scheme. This can be done through a small-signal analysis of the system, which will be an extended study of the proposed LVRT method.

D. Reactive Power Injection

Upon demands, reactive power can be injected in the case of grid faults, according to the control scheme in Fig. 2. In that

case, the maximum apparent power of the PV inverter denoted as S_{max} determines the capacity of reactive power [3]. This relationship is given as

$$|Q^*| \leq \sqrt{S_{max}^2 - (P^*)^2}. \tag{11}$$

Thus, if a reactive current is required during LVRT operation, the reactive power reference Q^* can be generated in consideration of (11) and then implemented in Fig. 2.

III. RESULTS

A. System Description

In order to verify the proposed LVRT control scheme, simulations have been carried out referring to Figs. 1 and 2. The system parameters are given in Table I. The environmental condition is considered as constant during LVRT (i.e., solar irradiance level: 1 kW/m² and ambient temperature: 25 °C). According to the PV panel parameters shown in Table II, the maximum power under this condition is 2.91 kW (there are three strings in parallel and each string has 15 panels in series). The corresponding voltage at the maximum power is 264 V (i.e., $v_{pv}^m = 15 \times 17.6$).

A PI controller is adopted to regulate the dc-link voltage as shown in Fig. 2, and a PR controller with an RC harmonic compensator has been used as the current controller. A second order generalized integrator based Phase Locked Loop (PLL) system has been employed to generate the virtual voltage $v_{g\beta}$ in respect to the real grid voltage v_g. The P&O MPPT algorithm has been adopted to track the maximum power of the PV panels. Controller parameters are provided in Table III.

TABLE I
PARAMETERS OF A TWO-STAGE SINGLE-PHASE GRID-CONNECTED PV SYSTEM (FIG. 1).

Parameter	Symbol	Value	Unit
Grid voltage amplitude	v_{gm}^0	325	V
Grid frequency	ω_g	314	rad/s
Boost inductor	L	2	mH
DC-link capacitor	C_{dc}	2200	μF
DC-link voltage reference	v_{dc}^*	450	V
	L_1	4.76	mH
LCL filter	C_f	4.28	μF
	L_2	4	mH
Boost converter switching frequency	f_b	16	kHz
Inverter switching frequency	f_{inv}	8	kHz
Sampling frequency	f_s	8	kHz

TABLE II
PARAMETERS OF THE SOLAR PV PANEL USED IN SIMULATIONS AT STANDARD TEST CONDITION (1 KW/M², 25 °C).

Parameter	Symbol	Value	Unit
Rated maximum power	P_{mpp}	65	W
Voltage at the maximum power	v_{mpp}	17.6	V
Current at the maximum power	i_{mpp}	3.69	A
Open-circuit voltage	v_{oc}	21.7	V
Short-circuit current	i_{sc}	3.99	A

Controller	Symbol	Value
DC-link PI controller	k_p	60
	k_i	250
PR controller	k_{pr}	20
	k_{ir}	4500
RC compensator gain	k_{rc}	6.5
MPPT control gain	k_m	0.00167
PV droop coefficient	k_{pv}	0.09
Active power droop coefficient	k_d	0.0317

B. Simulation Results

Firstly, the grid-connected PV system is controlled to always operate at unity power factor (i.e., without reactive power injection during LVRT). The simulation results are shown in Fig. 6, where as mentioned there is no reactive power injected in this case. At the beginning, the PV system is operating at the MPPT mode, and the steady-state duty-cycle should be $d_b = 1 - 264/450 \approx 0.41$, which can be read from Fig. 6. It means that the MPPT controller is properly designed and it can effectively track the maximum power before the voltage sag. Notably, during this operation period, the proposed LVRT scheme is already plugged-into the MPPT controller according to Fig. 4. It is thus demonstrated that the proposed LVRT controller will not affect the MPPT controller in the normal operation mode, where the voltage level deviation is almost null (i.e., $\Delta v_{gm} \approx 0$).

By monitoring the instantaneous grid voltage level estimated by the PLL system, the grid voltage fault can be detected. Once a grid voltage sag occurs, the output of the plug-in LVRT controller will increase the duty-cycle. Consequently, the PV voltage will move to the left side of the maximum power point in order to maintain the dc-link voltage level, which has been discussed previously. As a result, the PV output power is reduced. To verify this, a voltage fault has been enabled at a time instant of t_1, and it lasts for 200 ms. Fig. 6 shows the dynamic performance in the case of this fault. Observations from the grid voltage profile v_g in Fig. 6 indicate that the voltage amplitude drops to around $v_{gm} = 195$ V from its initial nominal value $v_{gm}^0 = 325$ V, corresponding to a voltage sag level of 0.4 p.u.. Obviously, it is verified that the single-phase two-stage grid-connected PV system shown in Fig. 1 with the proposed LVRT control scheme can ride-through this temporary grid fault. The duty-cycle is increased in the period of low grid voltage as analyzed above, which in return reduces the PV output power. Moreover, the operational mode change from MPPT to LVRT (or reversely) is accomplished within a few line cycles, indicating that the proposed LVRT scheme has a very fast dynamic. At the same time, it is found that the dc-link voltage v_{dc} has also been maintained around 450 V with an overshoot of about 5.6%.

Furthermore, seen from the grid-side, if the PV panels are still operating in the MPPT mode during the LVRT, the PV inverter will be overloaded (i.e., over-current) as mentioned
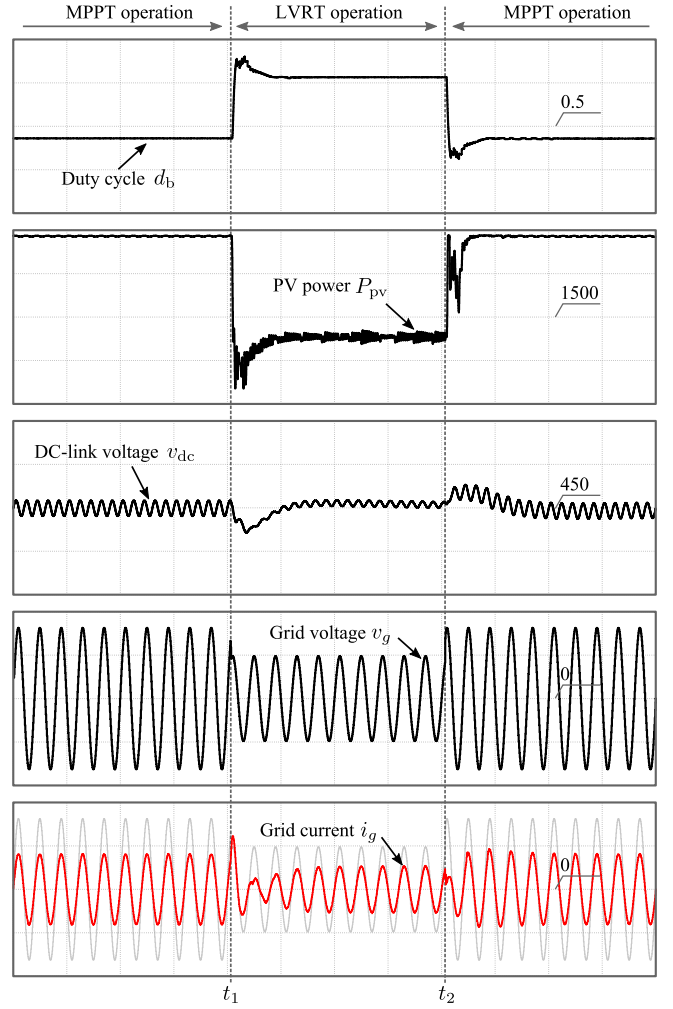

Fig. 6. Simulation results of the two-stage single-phase grid-connected PV system with the proposed LVRT control scheme under a grid voltage fault (voltage sag level: 0.4 p.u., that is, the amplitude residual voltage is 195 V): duty cycle d_b [0.25/div]; PV output power P_{pv} [750 W/div]; DC-link voltage v_{dc} [25 V/div]; grid voltage v_g [200 V/div]; grid current i_g [20 A/div]; time [50 ms/div]. No reactive current injection in this case.

above, since the voltage level is low. In contrast, when the proposed LVRT control scheme shown in Fig. 4 is plugged-in, the PV output active power P_{pv} has been effectively reduced to a certain level so that the PV inverter will not experience any severe over-current, as it is shown in Fig. 6. Also, it is stated above that there is no reactive power injection in this case, the grid current i_g and the grid voltage v_g are in phase under the grid fault. When the grid voltage recoveries, the system again operates at the MPPT mode.

In addition, it should be mentioned that, single-phase PV systems are commonly connected to low-voltage feeders, which are mainly resistive (i.e., with a high *R/X* ratio). Therefore, injecting reactive power to the grid may not contribute significantly to the grid voltage recovery. Nevertheless, the proposed LVRT scheme can also enable the injection of reactive power if demanded during fault ride-through, as it is demonstrated in Fig. 7. In this case, in order to prevent
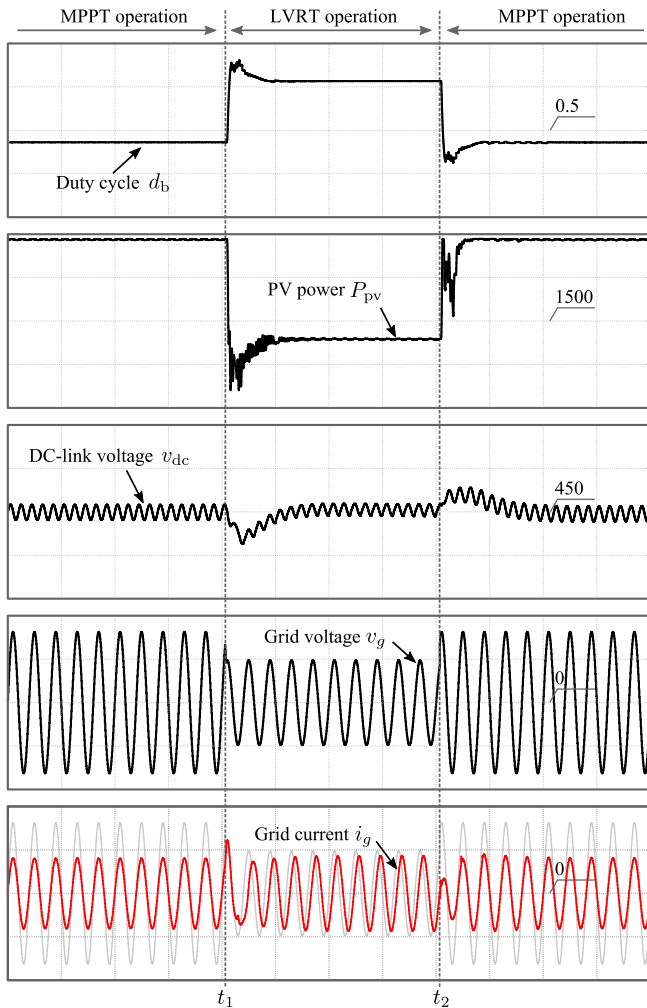
Fig. 7. Simulation results of the two-stage single-phase grid-connected PV system with the proposed LVRT control scheme under a grid voltage fault (voltage sag level: 0.4 p.u., that is, the amplitude residual voltage is 195 V): duty cycle d_b [0.25/div]; PV output power P_{pv} [750 W/div]; DC-link voltage v_{dc} [25 V/div]; grid voltage v_g [200 V/div]; grid current i_g [20 A/div]; time [50 ms/div]. An amount of reactive power is injected during the LVRT operation, where the grid current amplitude is kept the same as that before the grid fault.

the PV inverter from over-current shutdown, the grid current amplitude is maintained as it was (before the voltage sag). It can be seen in Fig. 7 that the PV system with the proposed LVRT scheme allows reactive power injection, since it is almost independent of the active power reduction of the PV panels. The dynamic of the system with the reactive power injection is also not comprised, as it is observed in Fig. 7.

C. Discussions

In order to better understand the dynamics of the system under LVRT, the operational trajectory of the PV panels of the grid-connected system is depicted in Fig. 8. It can be seen that from the MPPT to LVRT operation, there are periods of very low voltage and very low power (also can be observed in Figs. 6 and 7). This might be explained by the following. Typically, there is a capacitor at the output terminals of PV
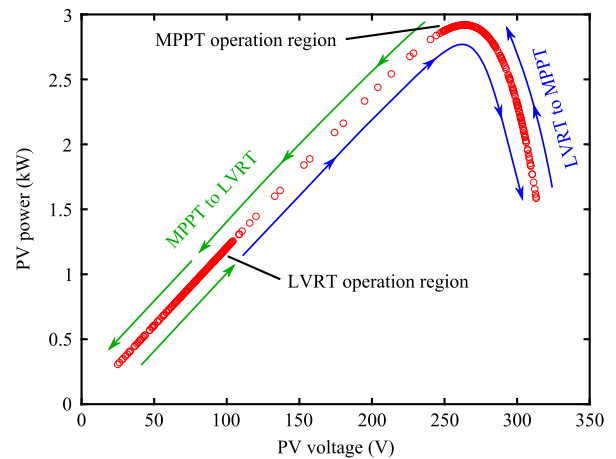

Fig. 8. Operational trajectory of the PV panels in the case of LVRT with the proposed control scheme.

panels (represented by C_{pv}). In the case of voltage sags, the duty-cycle d_b will experience a large step-up change, which will lead to a sudden drop in the PV voltage. The PV voltage change then creates an amount of energy at the capacitor C_{pv}. The energy will be gradually dissipated in the system, affecting the PV voltage profile. Similarly, when the grid voltage level comes to its nominal, a step-down change of the duty-cycle d_b occurs, forcing the PV operating point move to the high-voltage region (see Fig. 8). In this time period, the energy will be released gradually until the system reaches the maximum power point. In order to alleviate this impact, the PV output capacitor should not be too large, which is also valid in practical cases.

From the above simulations, it is known that the proposed LVRT scheme does not require to calculate the grid active power, but by monitoring the grid voltage amplitude, the PV output power is regulated. However, when the PV inverter is controlled by a droop controller, the calculation is inevitable. In that case, the active power droop coefficient k_d is readily available. Notably, the active power droop coefficient employed in this paper is not optimal, and it is related to the inverter system characteristics. Notice that the PV output power and the dc-link voltage contain double-line frequency components, a notch filter has been employed to mitigate these unwanted harmonics in this paper.

IV. CONCLUSIONS

In this paper, a cost-effective LVRT control scheme has been proposed for single-phase two-stage grid-connected PV systems, which can simply be plugged into a pre-designed MPPT controller, being easy for implementation. The proposed LVRT strategy is built upon the droop characteristics of PV systems (grid-side droop: active power and grid voltage level, PV-side inherent linear power-voltage droop: PV power and PV voltage). Hence, the plug-in LVRT enables seamless operation mode transitions, but also reactive power injection upon demands. Simulations on a 3-kW PV system have demonstrated the effectiveness of the proposal.

REFERENCES

[1] Fraunhofer Institute for Solar Energy Systems, "Recent facts about photovoltaics in Germany," *Tech. Rep.*, Apr. 22, 2016. Retrieved on July 21, 2016. Available at: https://www.ise.fraunhofer.de/en/publications.

[2] Y. Xue, K. C. Divya, G. Griepentrog, M. Liviu, S. Suresh, and M. Manjrekar, "Towards next generation photovoltaic inverters," in *Proc. ECCE*, pp. 2467–2474, Sept. 2011.

[3] Y. Yang, P. Enjeti, F. Blaabjerg, and H. Wang, "Wide-scale adoption of photovoltaic energy: Grid code modifications are explored in the distribution grid," *IEEE Ind. Appl. Mag.*, vol. 21, no. 5, pp. 21–31, Sept. 2015.

[4] M. Braun, T. Stetz, R. Bründlinger, C. Mayr, K. Ogimoto, H. Hatta, H. Kobayashi, B. Kroposki, B. Mather, M. Coddington, K. Lynn, G. Graditi, A. Woyte, and I. MacGill, "Is the distribution grid ready to accept large-scale photovoltaic deployment? state of the art, progress, and future prospects," *Progress in Photovoltaics: Research and Applications*, vol. 20, no. 6, pp. 681–697, 2012.

[5] B. Kroposki, "Can solar save the grid?" *IEEE Spectrum*, vol. 53, no. 11, pp. 42–47, Nov. 2016.

[6] Y. Yang, F. Blaabjerg, H. Wang, and M. G. Simes, "Power control flexibilities for grid-connected multi-functional photovoltaic inverters," *IET Renew.Power Gener.*, vol. 10, no. 4, pp. 504–513, Apr. 2016.

[7] Y. Bae, T. K. Vu, and R. Y. Kim, "Implemental control strategy for grid stabilization of grid-connected PV system based on German grid code in symmetrical low-to-medium voltage network," *IEEE Trans. Energy Convers.*, vol. 28, no. 3, pp. 619–631, Sept. 2013.

[8] J. L. Sosa, M. Castilla, J. Miret, J. Matas, and Y. A. Al-Turki, "Control strategy to maximize the power capability of pv three-phase inverters during voltage sags," *IEEE Trans. Power Electron.*, vol. 31, no. 4, pp. 3314–3323, Apr. 2016.

[9] C. Y. Tang, Y. T. Chen, and Y. M. Chen, "PV power system with multi-mode operation and low-voltage ride-through capability," *IEEE Trans. Ind. Electron.*, vol. 62, no. 12, pp. 7524–7533, Dec. 2015.

[10] G. Dötter, F. Ackermann, N. Bihler, R. Grab, S. Rogalla, and R. Singer, "Stable operation of PV plants to achieve fault ride through capability - evaluation in field and laboratory tests," in *Proc. PEDG*, pp. 1–8, Jun. 2014.

[11] X. Bao, P. Tan, F. Zhuo, and X. Yue, "Low voltage ride through control strategy for high-power grid-connected photovoltaic inverter," in *Proc. APEC*, pp. 97–100, Mar. 2013.

[12] H. C. Chen, C. T. Lee, P. T. Cheng, R. Teodorescu, and F. Blaabjerg, "A low-voltage ride-through technique for grid-connected converters with reduced power transistors stress," *IEEE Trans. Power Electron.*, vol. 31, no. 12, pp. 8562–8571, Dec. 2016.

[13] C. H. Benz, W. T. Franke, and F. W. Fuchs, "Low voltage ride through capability of a 5 kW grid-tied solar inverter," in *Proc. EPE/PEMC*, pp. T12–13–T12–20, Sept. 2010.

[14] G. Ding, F. Gao, H. Tian, C. Ma, M. Chen, G. He, and Y. Liu, "Adaptive dc-link voltage control of two-stage photovoltaic inverter during low voltage ride-through operation," *IEEE Trans. Power Electron.*, vol. 31, no. 6, pp. 4182–4194, June 2016.

[15] X. Zhao, J. M. Guerrero, M. Savaghebi, J. C. Vasquez, X. Wu, and K. Sun, "Low voltage ride-through operation of power converters in grid-interactive microgrids by using negative-sequence droop control," *IEEE Trans. Power Electron.*, vol. PP, no. 99, pp. 1–14, in press, DOI: 10.1109/TPEL.2016.2570204, 2016.

[16] Z. Shao, X. Zhang, F. Wang, R. Cao, and H. Ni, "Analysis and control of neutral-point voltage for transformerless three-level pv inverter in lvrt operation," *IEEE Trans. Power Electron.*, vol. PP, no. 99, pp. 1–13, in press, DOI: 10.1109/TPEL.2016.2565640, 2016.

[17] A. Sandali, T. Oukhoya, and A. Cheriti, "LVRT control strategy for PV grid connected system based on P-V optimal slope MPPT technique," in *Proc. IRSEC*, pp. 1–6, Dec. 2015.

[18] Y. Yang, F. Blaabjerg, and H. Wang, "Low-voltage ride-through of single-phase transformerless photovoltaic inverters," *IEEE Trans. Ind. Appl.*, vol. 50, no. 3, pp. 1942–1952, May 2014.

[19] H. Kobayashi, "Fault ride through requirements and measures of distributed PV systems in Japan," in *Proc. IEEE PES General Meeting*, pp. 1–6, Jul. 2012.

[20] N. P. Papanikolaou, "Low-voltage ride-through concept in flyback invert-erbased alternating current-photovoltaic modules," *IET Power Electron.*, vol. 6, no. 7, pp. 1436–1448, Aug. 2013.

[21] F. Blaabjerg, R. Teodorescu, M. Liserre, and A. V. Timbus, "Overview of control and grid synchronization for distributed power generation systems," *IEEE Trans. Ind. Electron.*, vol. 53, no. 5, pp. 1398–1409, Oct. 2006.

[22] K. Kawabe and K. Tanaka, "Impact of dynamic behavior of photovoltaic power generation systems on short-term voltage stability," *IEEE Trans. Power Syst.*, vol. 30, no. 6, pp. 3416–3424, Nov. 2015.

[23] N. A. Rahim, R. Saidur, K. H. Solangi, M. Othman, and N. Amin, "Survey of grid-connected photovoltaic inverters and related systems," *Clean Technol. Environ. Policy*, vol. 14, no. 4, pp. 521–533, 2012.

[24] Y. Yang and F. Blaabjerg, "Overview of single-phase grid-connected photovoltaic systems," *Electr. Power Compon. Syst.*, vol. 43, no. 12, pp. 1352–1363, 2015.

[25] K. Zhou, D. Wang, Y. Yang, and F. Blaabjerg, *Periodic Control of Power Electronic Converters*. Institution of Engineering & Technology, 2017.

[26] H. Liu, P. C. Loh, X. Wang, Y. Yang, W. Wang, and D. Xu, "Droop control with improved disturbance adaption for a PV system with two power conversion stages," *IEEE Trans. Ind. Electron.*, vol. 63, no. 10, pp. 6073–6085, Oct. 2016.

[27] H. Liu, Y. Yang, X. Wang, P. C. Loh, F. Blaabjerg, W. Wang, and D. Xu, "An enhanced dual droop control scheme for resilient active power sharing among paralleled two-stage converters," *IEEE Trans. Power Electron.*, vol. PP, no. 99, pp. 1–14, in press, 2017.

[28] E. Koutroulis, K. Kalaitzakis, and N. C. Voulgaris, "Development of a microcontroller-based, photovoltaic maximum power point tracking control system," *IEEE Trans. Power Electron.*, vol. 16, no. 1, pp. 46–54, Jan. 2001.

[29] A. K. Abdelsalam, A. M. Massoud, S. Ahmed, and P. N. Enjeti, "High-performance adaptive perturb and observe MPPT technique for photovoltaic-based microgrids," *IEEE Trans. Power Electron.*, vol. 26, no. 4, pp. 1010–1021, Apr. 2011.

[30] N. Femia, G. Petrone, G. Spagnuolo, and M. Vitelli, "Optimization of perturb and observe maximum power point tracking method," *IEEE Trans. Power Electron.*, vol. 20, no. 4, pp. 963–973, Jul. 2005.

[31] H. Xin, Z. Lu, Y. Liu, and D. Gan, "A center-free control strategy for the coordination of multiple photovoltaic generators," *IEEE Trans. Smart Grid*, vol. 5, no. 3, pp. 1262–1269, May 2014.

[32] J. M. Blanes, F. J. Toledo, S. Montero, and A. Garrigs, "In-site real-time photovoltaic I-V curves and maximum power point estimator," *IEEE Trans. Power Electron.*, vol. 28, no. 3, pp. 1234–1240, Mar. 2013.